Chapter 1

Correlation and scattering analysis of passive seismic data

In this chapter, I use two methods to attempt to image subsurface layers from passive data. The first is a correlation-based approach. My advisor Jon Claerbout hypothesized that the crosscorrelation of two seismic noise data traces should resemble what we would record from a shot at one trace location and a receiver at the other. This idea is illustrated in Figure 1.1. For each source-receiver offset, there is a certain arrival direction for incident plane waves that will follow the source-receiver raypath. If that incident plane wave is present, then that segment of the traveltime hyperbola will be present.

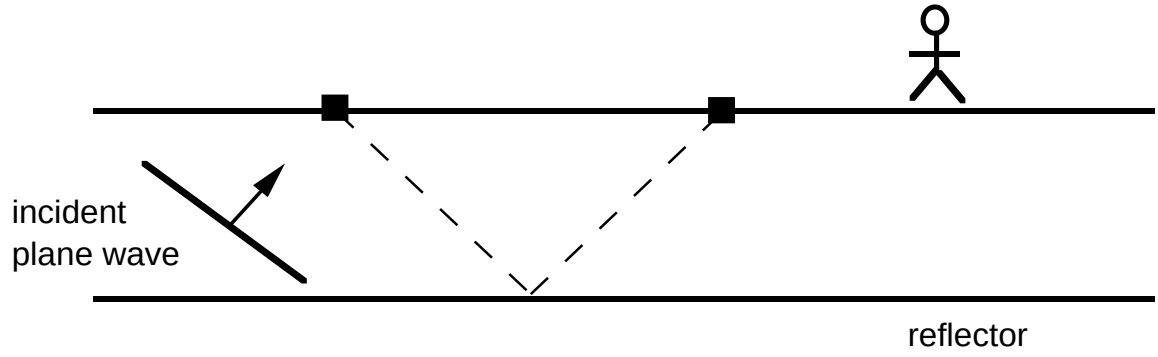

Figure 1.1: Illustration of crosscorrelation scheme. For each source-receiver separation, there is one plane wave angle of incidence that will follow the source-receiver raypath shown. If this incident plane wave is present, then, correlating traces recorded at the two locations should reveal a positive correlation at the corresponding time lag. Assuming a flat subsurface layer allows us to sum together all source-receiver pairs have the same separation. corr-corr [NR]

A synthetic data example illustrates how this method works. In Figure 1.2, three synthetic datasets are shown. One contains a single dipping plane wave, another five plane waves, and the third contains one hundred plane waves. The dips of the plane waves have been chosen randomly. A different arbitrary source signature has

been convolved onto each event, by choosing a random source amplitude for each frequency component. This simulates the random dips and source signatures that we might expect to encounter in the ambient noise field.

To process the data, we crosscorrelate each trace against all other traces. This gives, in effect, the traveltime as a function of trace-to-trace offset. We sort the traces according to this offset, and perform a partial stack into a number of offset bins. This gives a profile, on which we should see the normal moveout hyperbola. In Figure 1.3, with a single plane wave, only a single offset of that hyperbola would be present. But as we add more plane waves, we illuminate more source-receiver offsets. In Figure 1.4, five different incident angles are present, and an event at the right zero-offset time having moveout that appears to be hyperbolic is visible. This event is more sharply defined in Figure 1.5, with one hundred different plane waves present.

Real data results for a number of records are shown in Figures 1.6 through 1.14. In most cases there is little evidence of the sort of hyperbolic events we would expect, and those features that might be these events do not seem consistent between records as we would expect.

The lack of such hyperbolic features is disappointing. However, the success in the synthetic case depended partly on the presence of a flat subsurface layer. We know that the geology of our site, which is in close proximity to the San Andreas fault, is quite complex. This method should be tested in an area with known flat layers, to see if it can be beneficial.

1.1 Autocorrelation analysis

Another correlation-based approach would be to simply autocorrelate the traces. For a plane-layered earth, autocorrelation of the traces should reveal the subsurface impedance structure, as given by the Kunetz-Claerbout relation.

This analysis was also performed on the passive data. The results are not shown here because while there was some coherency in the autocorrelations from trace to trace in a given data record, there was little agreement between records. This suggests that none of the coherent events observed in the autocorrelations are related to the subsurface geology.

1.2 Scattering analysis

The second technique is a scattering-based approach. Here we picture the subsurface near the array as a three dimensional grid of possible source locations, as shown in Figure 1.15. At each of these locations, given an estimate of the necessary stacking velocity, we stack or compute semblance along the moveout trajectory.

Scatterers near the array should act as secondary sources. While we can't image these sources with conventional migration since we don't know the time at which they

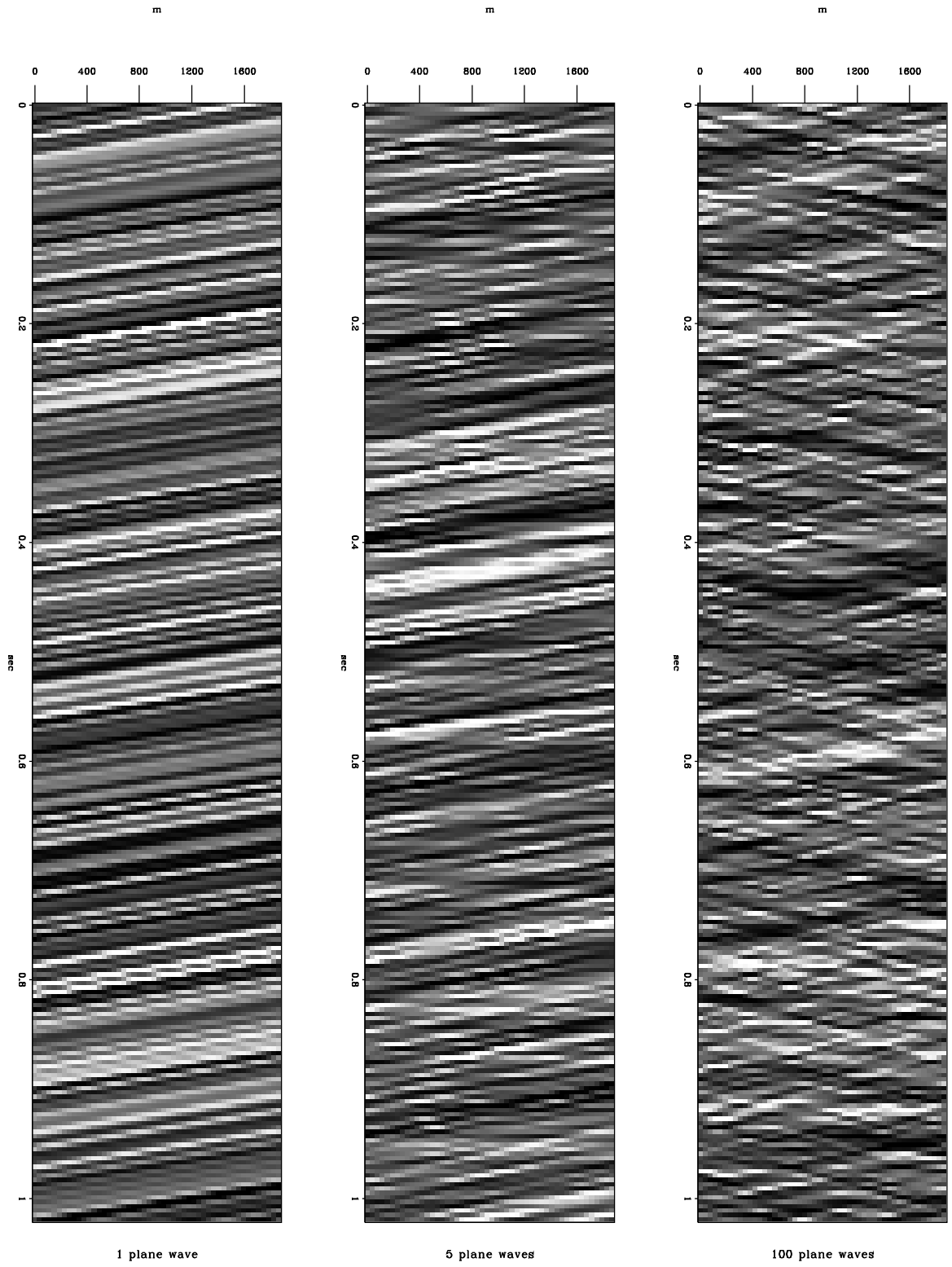

Figure 1.2: Synthetic datasets contains 1, 5, and 100 plane waves with randomly selected dips and source signatures. corr-pmod [ER]

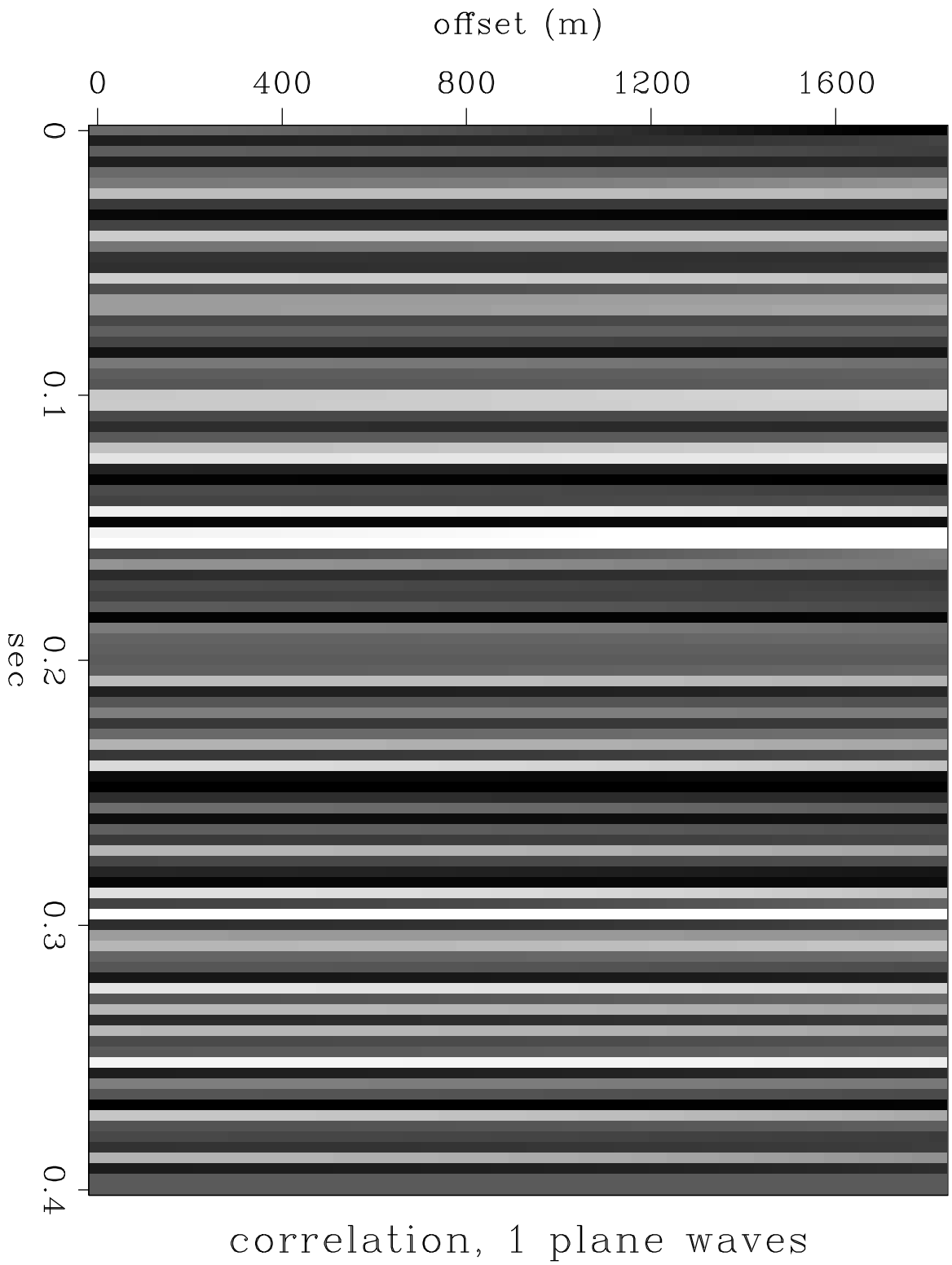

Figure 1.3: Result of crosscorrelation processing for a single dipping plane wave. Each trace is correlated against every other trace, and then the traces are binned and partially stacked according to the inter-trace distance. corr-pst.1 [ER]

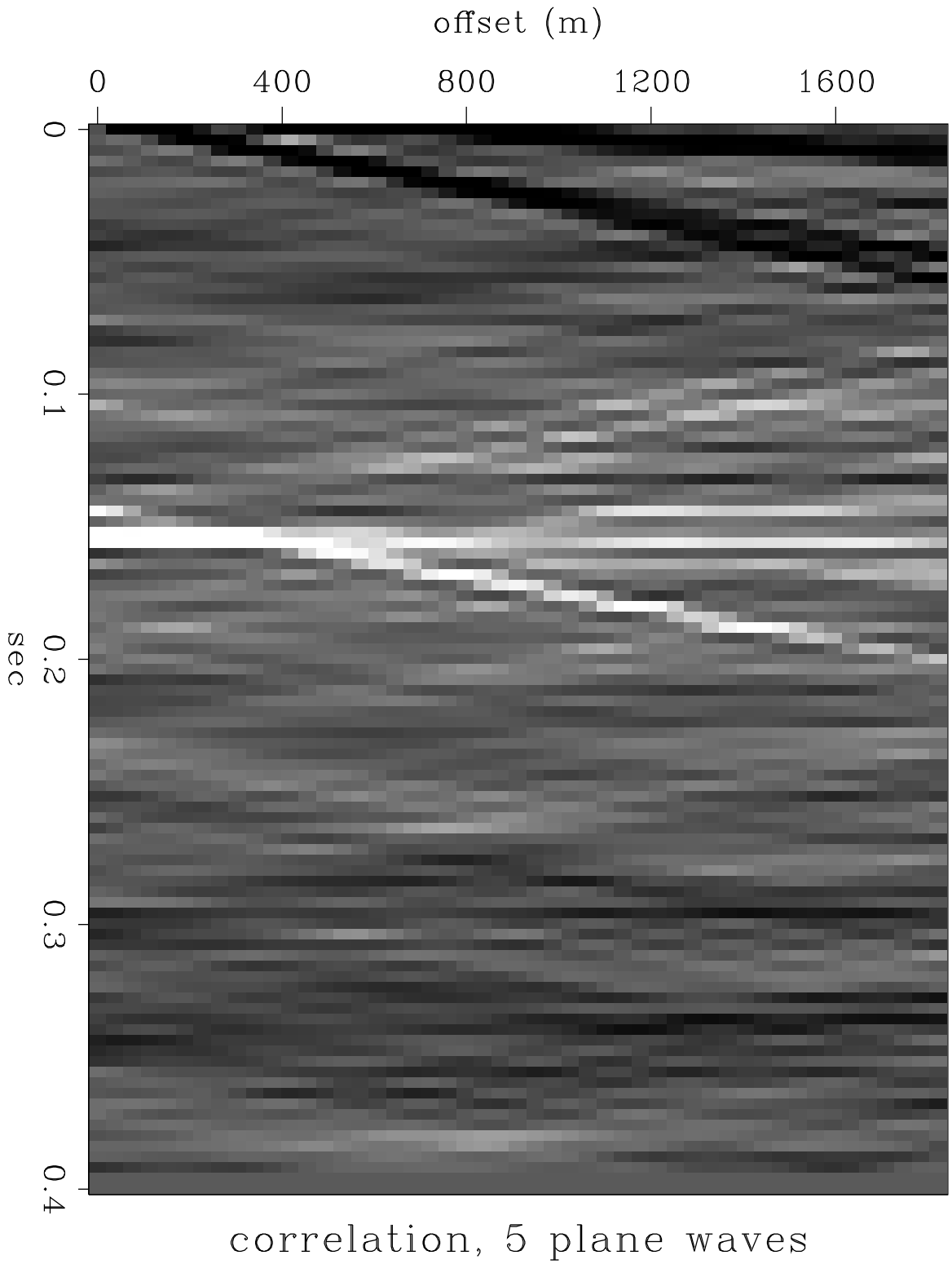

Figure 1.4: Result of crosscorrelation processing for the data containing five dipping plane waves. corr-pst.5 [ER]

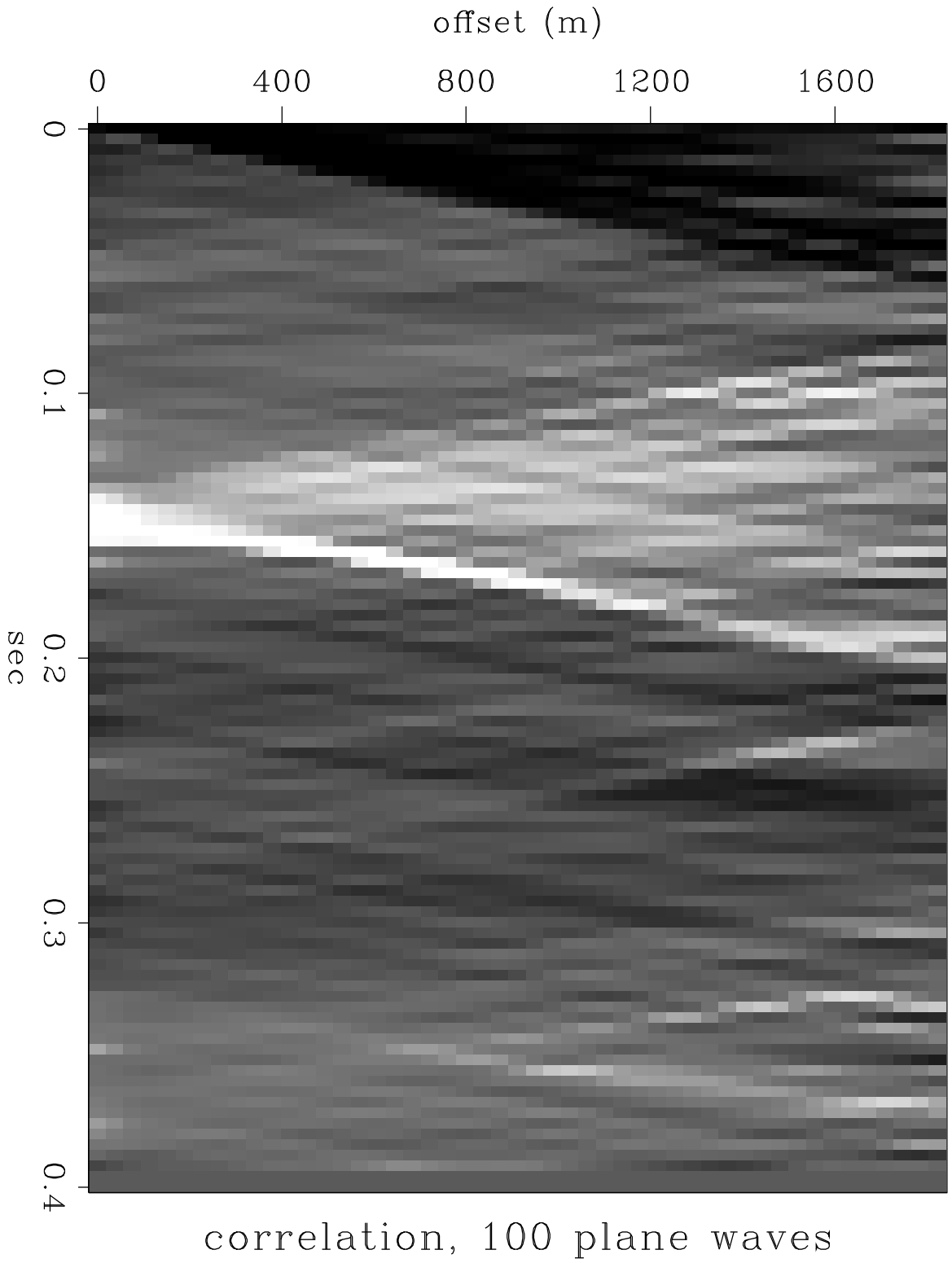

Figure 1.5: Result of crosscorrelation processing for the data containing one hundred dipping plane waves. An event can be seen at the proper zero-offset time (0.15 seconds) having roughly hyperbolic moveout. corr-pst.100 [ER]

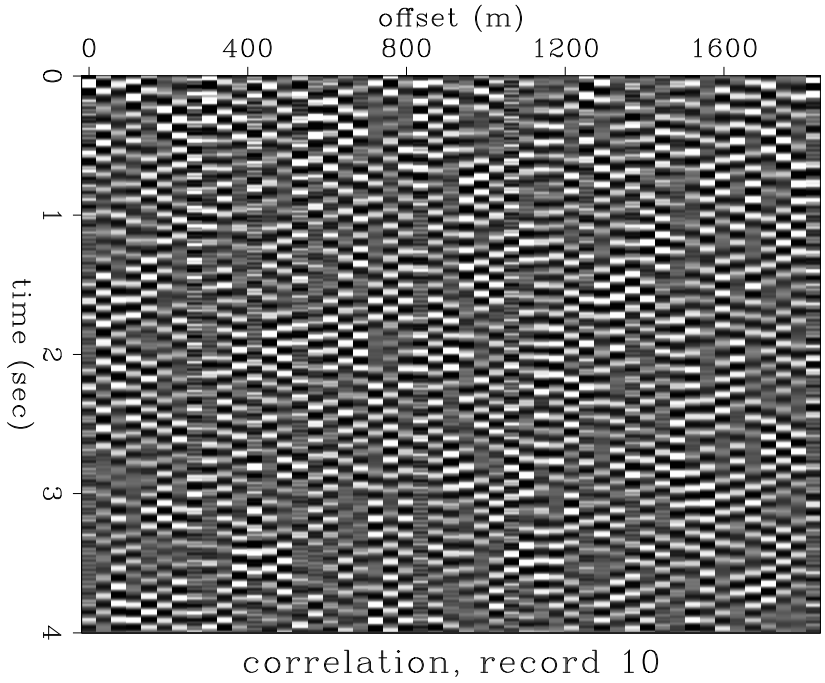

Figure 1.6: Result of crosscorrelation processing for data record 10. [ER]

corr-pstack.10

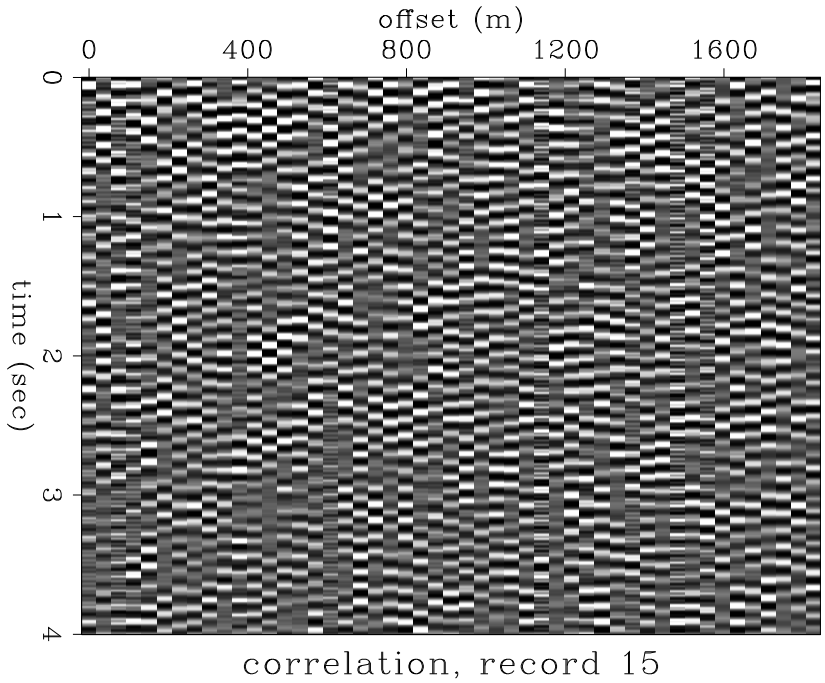

Figure 1.7: Result of crosscorrelation processing for data record 15. [ER]

corr-pstack.15

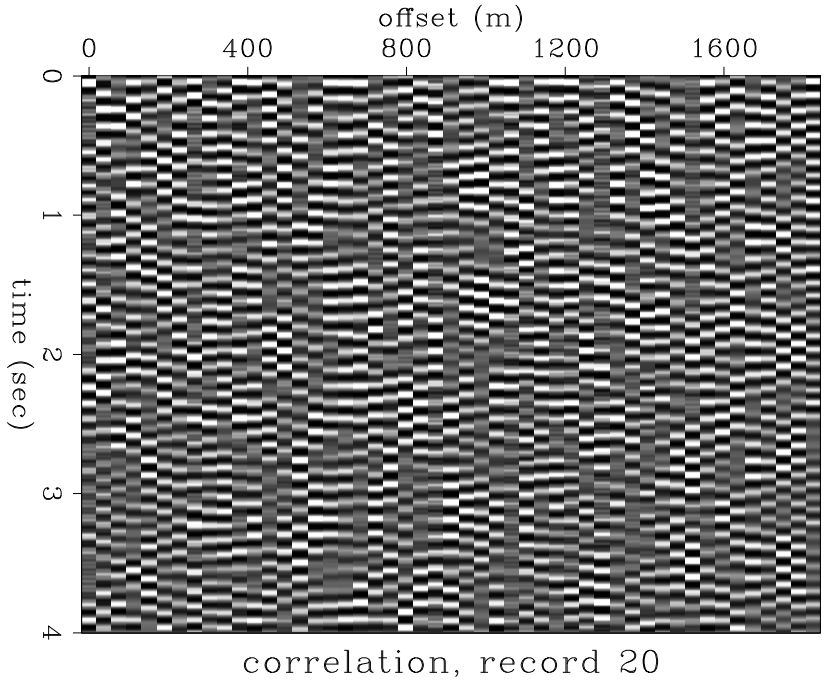

Figure 1.8: Result of crosscorrelation processing for data record 20. [ER]

corr-pstack.20

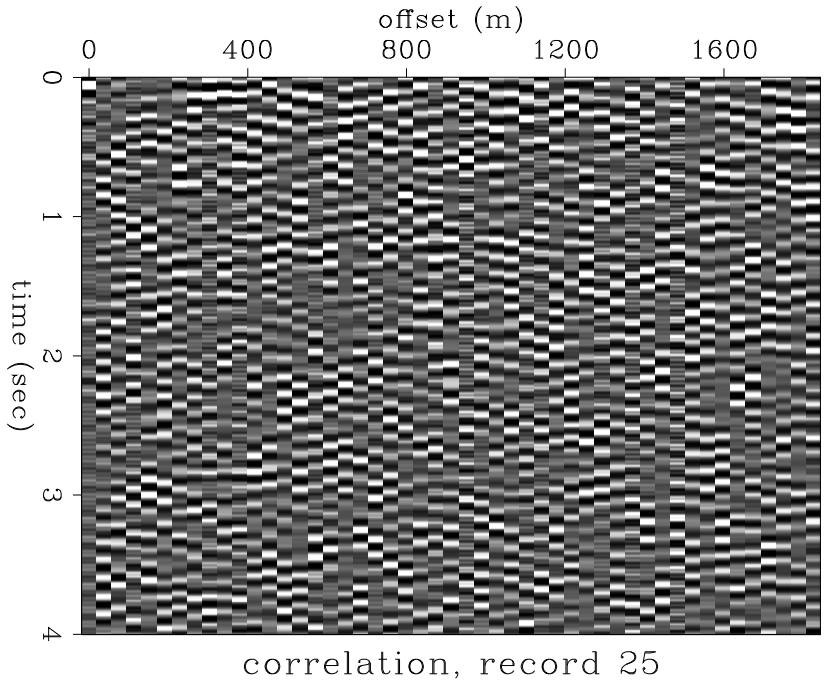

Figure 1.9: Result of crosscorrelation processing for data record 25. [ER]

corr-pstack.25

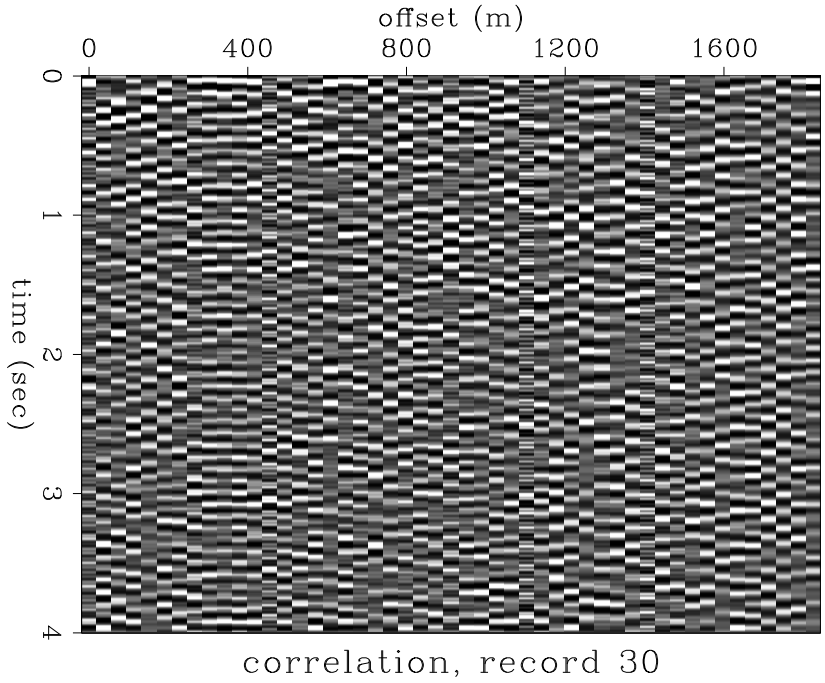

Figure 1.10: Result of crosscorrelation processing for data record 30. corr-pstack.30 [ER]

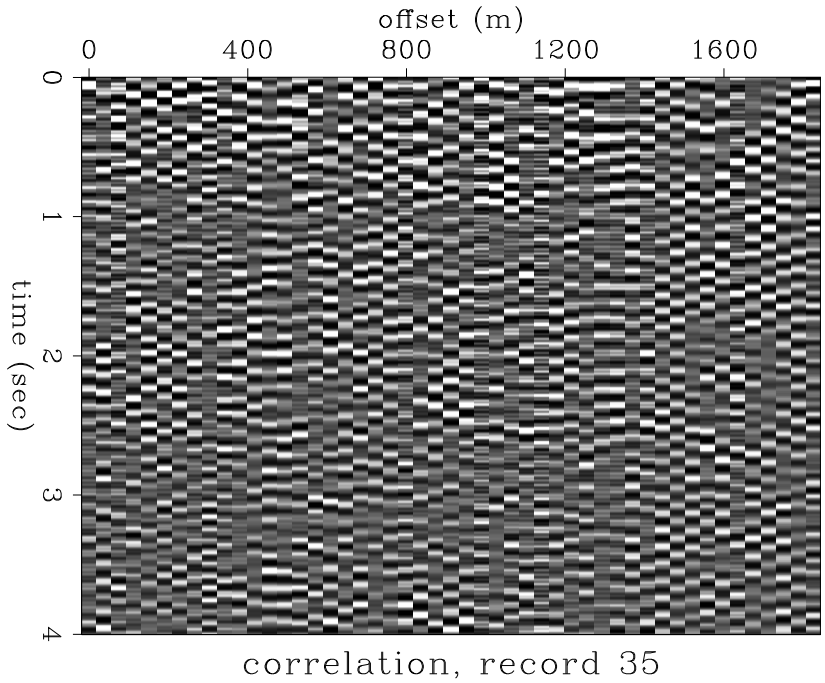

Figure 1.11: Result of crosscorrelation processing for data record 35. corr-pstack.35 [ER]

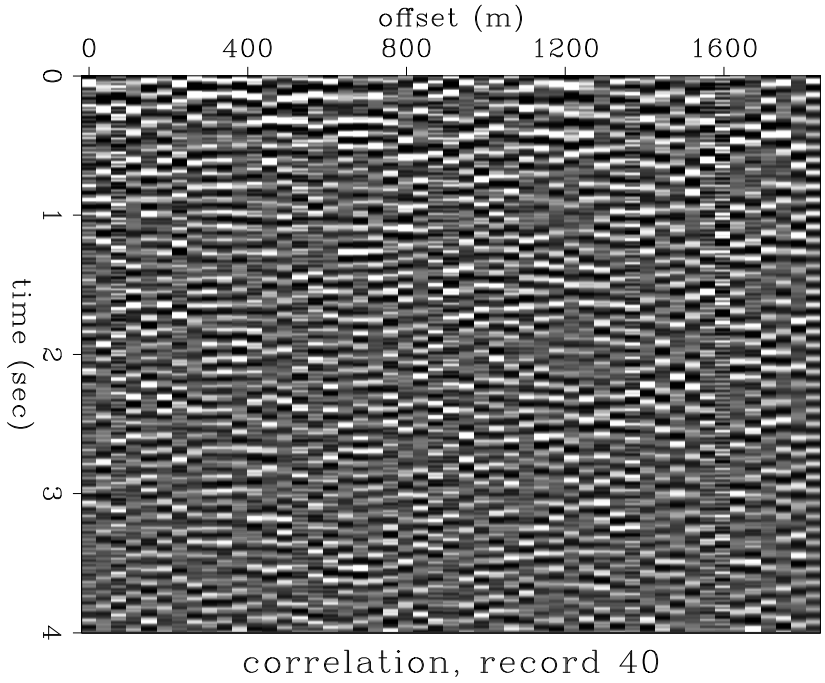

Figure 1.12: Result of crosscorrelation processing for data record 40. [ER]

corr-pstack.40

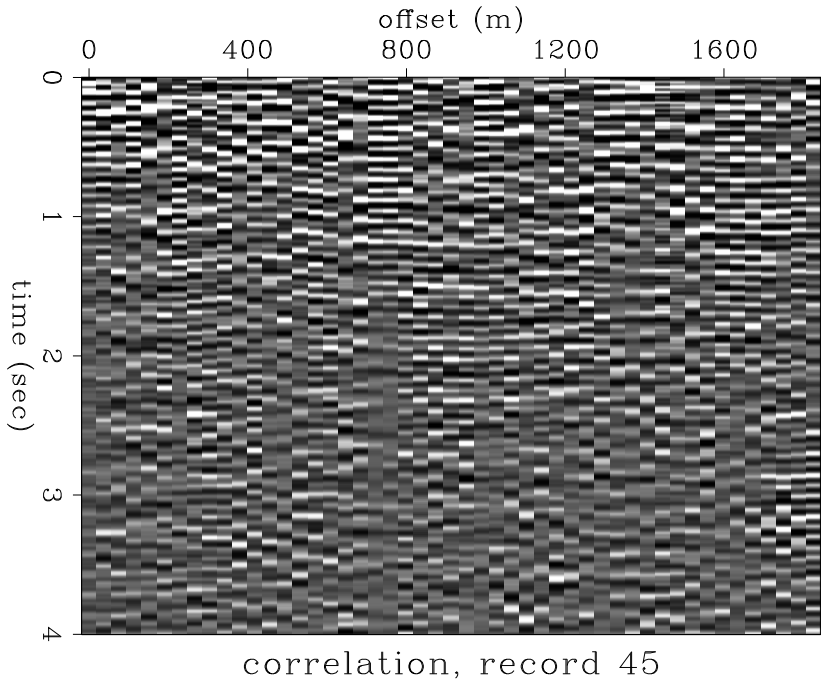

Figure 1.13: Result of crosscorrelation processing for data record 45. [ER]

corr-pstack.45

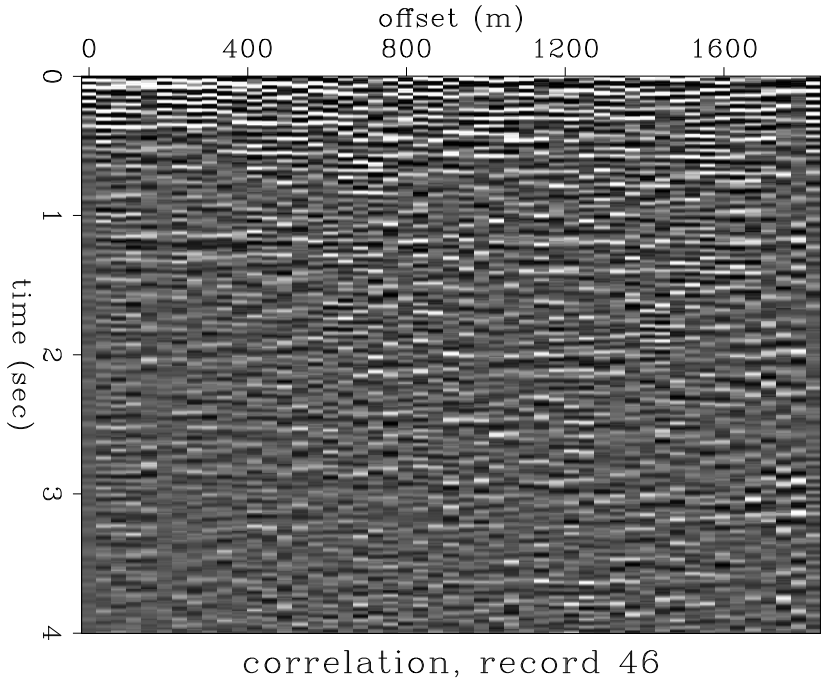

Figure 1.14: Result of crosscorrelation processing for data record 46. corr-pstack.46 [ER]

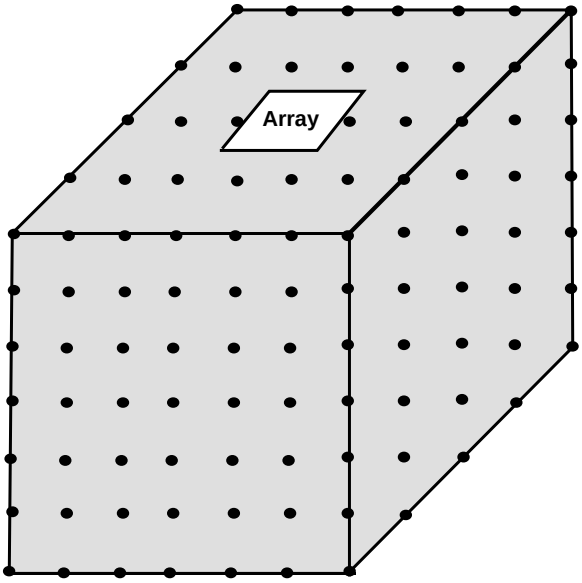

Figure 1.15: Scattering approach. A 3-D grid of possible source locations is constructed for the subsurface near the array. At each, data are stacked (or semblance is computed) along the appropriate moveout trajectory to search for sources. corr-scatter [NR]

"explode", we should be able to see in the data the moveout patterns that identify the source location.

A similar scheme was used by Troitskiy and Nikolaev (**?**) to image scatterers using teleseismic data *and* ambient noise data with the NORSAR array.

We create a 3-D grid of possible scatterer locations in the subsurface. For each location, we find the moveout trajectory for energy coming from that point, and compute semblance over time along this trajectory in our data. We can then look at the average semblance over time, or the maximum semblance observed over all times, to get an idea of the scatterers that may lie in the subsurface.

An important first question is, given the size of our array, how far away can scatterers be identified as such? The limited size of the array will make it impossible to see any moveout for events coming from scatterers beyond a certain distance. Beyond this distance, scattered energy will be indistinguishable from plane waves. Troitskiy and Nikolaev were using the NORSAR array, 110 km across, and was therefore theoretically able to image very deep structures. Our array is only 500 meters across, so our scattering analysis will be more localized. Figure 1.16 shows the moveout across the array for a scattered event versus distance of the scatterer from the array. This figure assumes a constant velocity of 2000 meters/sec, a very favorable choice. For higher velocities the dropoff will be sharper. The time difference drops to less than four milliseconds at around 5 kilometers from the array, so our scattering analysis definitely cannot go beyond that point. I have chosen one kilometer as an upper bound in the analysis that follows, to avoid coming too close to the limit.

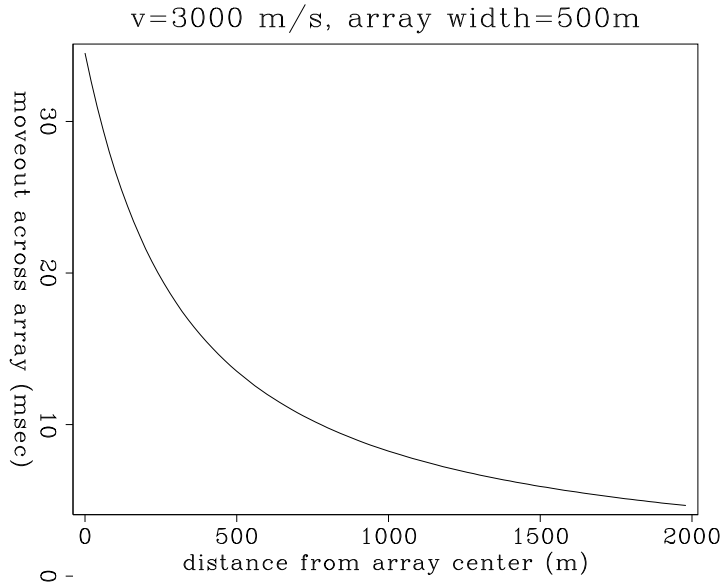

Figure 1.16: Moveout observable across our array for a scattering event as a function of scatterer distance from the array. Beyond about 5 kilometers the observable moveout drops to less than the time sampling interval, so scattered events will be indistinguishable from plane waves. corr-tdif [ER]

Figure ?? shows the image that is obtained for the $z = 0$ depth level when this scattering algorithm is applied to portions of several different nighttime and daytime records. The x and y dimensions of the grid of scattering locations shown are three times the size of the survey. Thus points up to 750 meters from the array center are shown in this plot. The dominant features in this plot are the radial streaks. These are due to the fact that as we get further from the array center, our summation path becomes flatter and flatter. Eventually we reach the point where we are summing along a plane wave path, and from there out we would just get a radial streak.

Figures ?? and ?? show the results for depths of 500 and 1000 meters. A feature worth noting in all of these is the general agreement among the daytime blast records, and among the nighttime records, but not between the two groups. The reason for this is that what we are seeing when we sum along these hyperbolic paths is, predominantly, plane wave energy, which was quite different during day and night recording periods. In Figure ??, I've performed the same computation as for Figure ??, but I've summed along plane wave paths rather than hyperbolic paths. The fact that these two plots are quite similar is disappointing; it means that the algorithm is seeing mainly plane wave energy imperfectly stacked along hyperbolic paths, rather than scattered energy.

If we are to see scattered energy, probably it is necessary to filter out the strong plane waves present throughout our dataset.

For the most part, I believe that what we are seeing with this analysis is plane wave energy stacking is somewhat because its trajectory is close enough to that being used for scatterers. I base this conclusion on the fact that most features track outward in radially from the center of the zero depth plot. The passive data seem to be dominated by events coming from the far field. Some technique that removes plane waves might allow us to do a better job of scattering analysis. But this method is very useful in the drill bit case described in the following chapter.

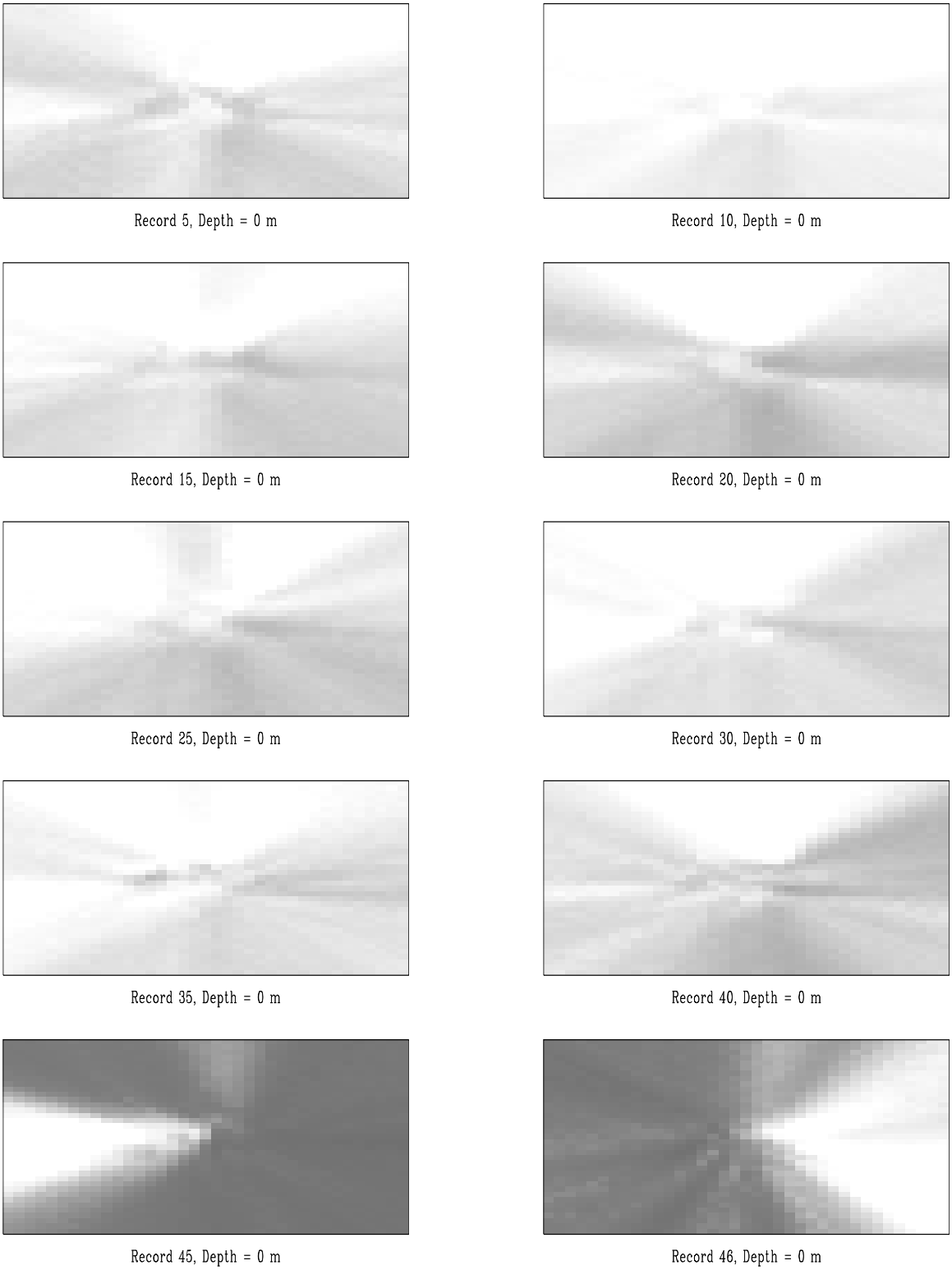

Figure 1.17: Semblance measure of scatterer strength as a function of position for a depth of 0 meters. The different frames correspond to different recording periods. The top four panels are nighttime records; the bottom four are daytime records. Of these, all but record 45 contain blasts. These plots cover a 1500 meter square area centered around the array. corr-scatp.0 [ER]

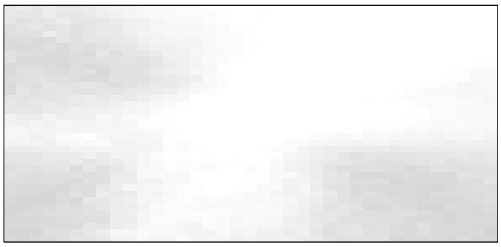

Record 5, Depth = 500 m

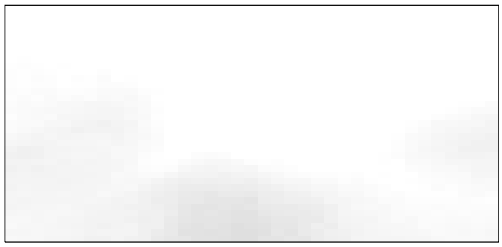

Record 10, Depth = 500 m

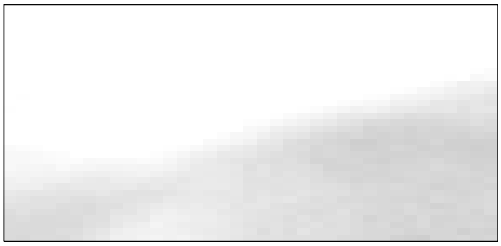

Record 15, Depth = 500 m

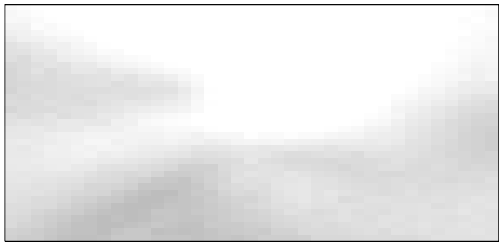

Record 20, Depth = 500 m

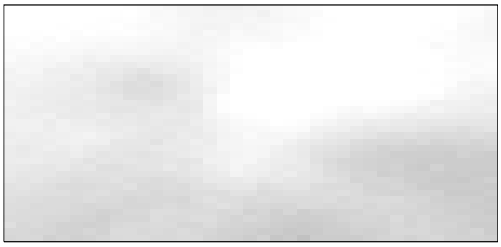

Record 25, Depth = 500 m

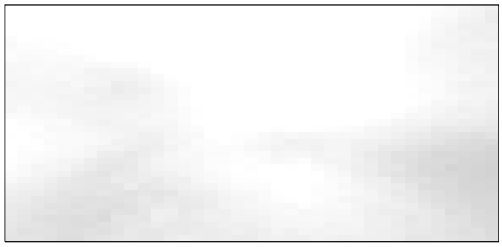

Record 30, Depth = 500 m

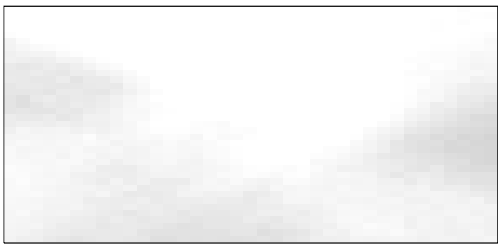

Record 35, Depth = 500 m

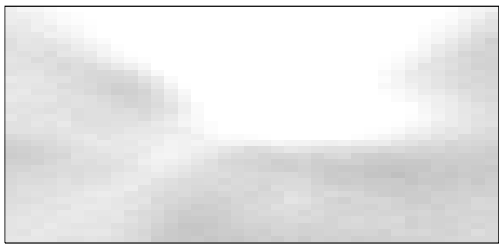

Record 40, Depth = 500 m

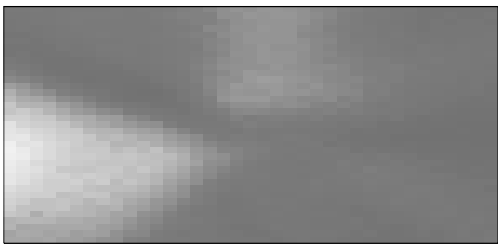

Record 45, Depth = 500 m

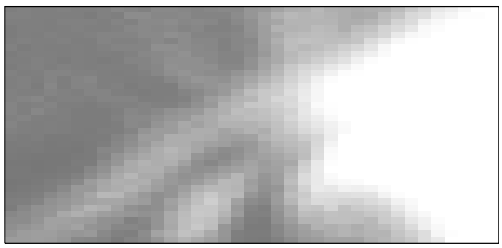

Record 46, Depth = 500 m

Figure 1.18: Same as Figure **??** but for a depth of 500 meters. corr-scatp.500 [ER]

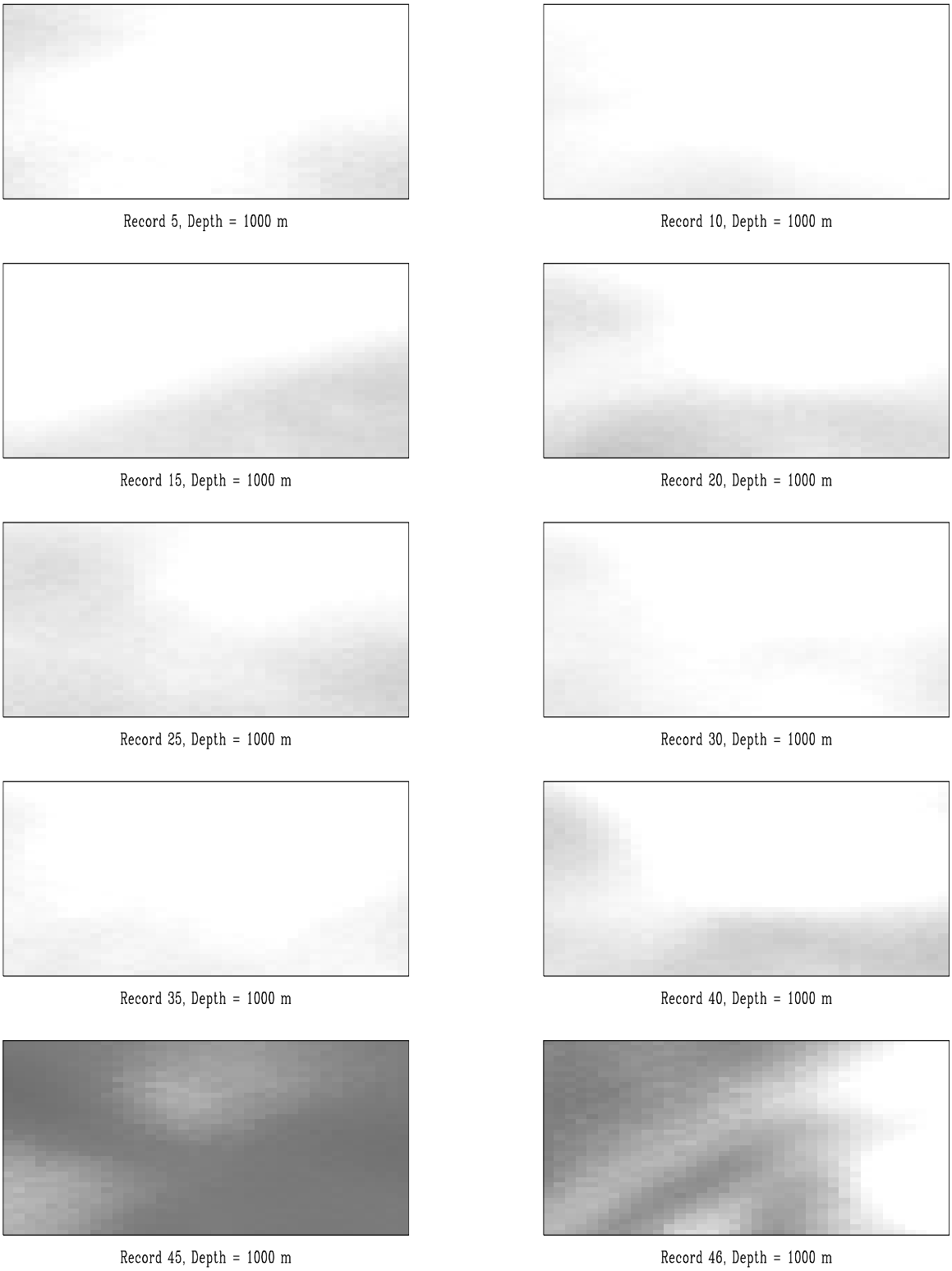

Figure 1.19: Same as Figure **??** but for a depth of 1000 meters. corr-scatp.1000 [ER]